Scientific Research Publishing

Materials Sciences and Applications, 2024, 15, 572-586
https://www.scirp.org/journal/msa
ISSN Online: 2153-1188
ISSN Print: 2153-117X

Accurate Control of Oxide Ions Content for Corrosion Studies: Application to SS316L and Its Alloying Elements in Molten LiCl-KCl

Thibaut Fourès[1], Mathieu Gibilaro[1*], Laurent Massot[1], Elisa Capelli[2], Bertrand Morel[2], Pierre Chamelot[1]

[1]Laboratoire de Génie Chimique, Université de Toulouse, Toulouse, France
[2]Orano, Châtillon, France
Email: *gibilaro@chimie.ups-tlse.fr

How to cite this paper: Fourès, T., Gibilaro, M., Massot, L., Capelli, E., Morel, B. and Chamelot, P. (2024) Accurate Control of Oxide Ions Content for Corrosion Studies: Application to SS316L and Its Alloying Elements in Molten LiCl-KCl. *Materials Sciences and Applications*, **15**, 572-586.
https://doi.org/10.4236/msa.2024.1512038

Received: November 14, 2024
Accepted: December 28, 2024
Published: December 31, 2024

Abstract

The aim of this work was to study the influence of oxide ions concentration on the stability of 316L stainless steel and its alloying compounds (chromium, iron, nickel and molybdenum) in molten LiCl-KCl-Li_2O at 550˚C. An *in-situ* oxide ions titration method using square wave voltammetry was developed to quantify oxide ions, to accurately control the experimental conditions. The influence of oxide ions concentration was then studied by linear sweep voltammetry and long-term immersions followed by SEM-EDS analysis on pure elements and SS316L. Results showed that chromium was stabilized in presence of O^{2-}, iron was dissolved independently of $[O^{2-}]$, nickel was resistant to corrosion and molybdenum, which was stable in oxide-free media, was found reactive towards O^{2-}. On SS316L, a passivation layer was observed and an enriched chromium-oxygen layer was observed by SEM-EDS. Almost all the iron was dissolved and a small depletion of molybdenum was visible while nickel remained resistant to corrosion. Linear sweep voltammetry studies were consistent with SEM-EDS analysis and each alloying compound exhibited a similar behaviour in the SS316L as its pure form.

Keywords

Chromium, Iron, Nickel, Molybdenum, Molten Salts, SS316L Stainless Steel, Oxide Ions

1. Introduction

Molten salts solvents have been proposed as fuel and coolant for next-generation molten salt reactor concepts. They are able to reduce the amount of spent nuclear

fuel produced during energy production, but one of the key challenges is the materials compatibility with the molten salt medium [1].

The first studies on molten salt reactors were conducted at Oak Ridge National Laboratory (ORNL) to design a nuclear powered aircraft engine in molten fluoride medium (Aircraft Reactor Experiment, T = 860˚C) [2]. Preliminary corrosion studies were first conducted on commercial alloys: Inconel 600, a Ni-based alloy with mainly chromium (15%) and iron (7%), showed the best corrosion resistance [3]. The aircraft reactor experiment was then conducted with this alloy as structural material and post operation salt analysis showed a chromium presence in the salt coming from Inconel 600 [4]. This led to the development of Hastelloy N, with an optimised composition to better resist corrosion, irradiation and high temperature in molten fluorides [5].

For the past decades, an increasing interest has shown in molten chloride fast reactors. Several research programs were launched, such as Moltex [6] and Dual Fluid Reactor [7] in Great-Britain and Germany respectively and the Terrapower project in the USA [8]. Despite this rise of interest, no resistant enough material was identified for molten chloride medium. Many authors are still discussing the influence of experimental parameters (impurities, atmosphere…) on corrosion performance and antagonistic results can be found.

For instance, chromium influence on corrosion as alloying compound is still under investigation. Slusser *et al.* studied corrosion performance of nickel/chromium and iron/chromium alloys in oxide ions rich nitrate-nitrite salts at 510˚C - 705˚C [9] and concluded that nickel alloys with high chromium content performed the best. On the other hand, Ding *et al.* [10] studied the corrosion behaviour of SS310, Inconel 800H and Haynes C-276 in an oxide ions free NaCl-KCl-$MgCl_2$ at 700˚C under an argon atmosphere. A Cr preferential dissolution was observed and alloys with higher Cr content were less resistant to corrosion. Oxide ions have thus an important impact on alloy behaviour in molten salt media.

In molten chloride melts, oxide ions come from pre-fusion moisture or from the atmosphere. It was for instance demonstrated on Mo element that atmosphere has an influence on metal stability. Sun *et al.* [11] observed under N_2 atmosphere that Mo was crucial to enhance corrosion resistance of Ni-based alloys in NaCl-KCl-$MgCl_2$ (33–21.6–45.4 mol%) at 700˚C. On the other hand, Shankar *et al.* [12] conducted corrosion studies under air on nickel-based alloys in molten LiCl-KCl eutectic salt at 400˚C, 500˚C and 600˚C and observed a higher corrosion rate for alloys containing Mo. The atmosphere is thus a crucial experimental parameter regarding Mo stability in the alloy. Moreover, Ishitsuka *et al.* [13] demonstrated that Mo metal was spontaneously oxidized into MoO_3 in presence of oxide ions in NaCl–KCl at 550˚C under N_2 atmosphere. Then, Volkovicha *et al.* [14] demonstrated that MoO_3 was unstable in NaCl-KCl medium due to its reactivity with chloride media, forming a volatile molybdenum oxychloride following Equation (1):

$$2MoO_3 + 2NaCl = MoO_2Cl_2 + Na_2MoO_4 \quad (1)$$

To resume, Mo is stable under Ar atmosphere (without oxide ions) and is oxidised under air (in presence of O^{2-}). The control of experimental conditions, both atmosphere and oxide ions content, is thus essential when performing corrosion tests.

The atmosphere above the salt is easy to monitor (air-tight cell, gas bottle…) whereas the oxide ions concentration is not. Indeed, the literature shows that O^{2-} presence is a critical parameter but its content in the salt is never quantified. Thus, the goal of this work is to propose an in-situ O^{2-} titration method, to precisely govern our operating conditions.

Then, the influence of oxide ions concentration on the corrosion behaviour of SS316L and its main alloying elements under an inert Ar atmosphere was investigated. An oxide ions titration technique using square wave voltammetry, inspired by earlier works in house on fluoride medium [15], was developed in molten chlorides to ensure precise control of the experimental conditions. Using linear sweep voltammetry and immersions followed by SEM observations, studies of the influence of oxide ions on pure metals (Cr, Fe, Ni and Mo) and SS316L were conducted.

2. Material and Methods

2.1. The Cell

A vitreous carbon crucible was placed in a cylindrical vessel made of refractory steel, closed to the top by a stainless-steel lid cooled by circulating water. The walls of the vessel were protected from chloride vapours by a graphite liner. The atmosphere of the cell was argon gas (99.995% purity, Linde). Heating was ensured by a programmable furnace and temperature was measured by a chromel-alumel thermocouple.

2.2. The Electrolyte

The electrolytic bath consisted of an eutectic mixture (58.2 mol.% - 41.8 mol.%) of LiCl (Sigma Aldrich, purity 99.98%) and KCl (Fox Chemicals, purity 99.99%). Li_2O (Fox chemicals, purity 99.9%) was used as a solute to target desired O^{2-} concentrations. All salts and solutes were stored in a glovebox under an argon atmosphere.

2.3. Materials and Electrodes

A classical three-electrode set-up was used for electrochemical measurements.

Working electrodes (WE) were made of metallic wires or cylindrical metallic pieces. Stainless steel 316L (69Fe-18Cr-10Ni-3Mo) and its main components were chosen for this study and supplied by Goodfellow. Table 1 gathers the shape and purity of each metal and alloy used in this study.

For electrochemical measurements a tungsten counter-electrode (CE) was used. It was ensured that the immersed surface area of the CE was greater than the WE one. The pseudo-reference electrode was a two millimeter diameter glassy carbon

Table 1. Material shape and purity.

Material	Shape	Purity
Cr	Cylindrical rod (2 mm diameter)	99.7%
Fe	Wire (1 mm diameter)	99.99%
Mo	Wire (1 mm diameter)	99.99%
W	Wire (0.5 mm diameter)	99.95%
SS316L	Wire (1 mm diameter)	-

rod. A 316L stainless steel plate was also used for the long-term immersion test.

2.4. Electrochemical and Analytical Techniques

Linear sweep voltammetry, square wave voltammetry and galvanostatic electrolysis were performed with an Autolab PGSTAT302N controlled by the software Nova 2.1.5.

The immersed samples were embedded in a conductive resin and polished to be further analysed by Scanning Electron Microscopy (SEM) coupled with Electron Dispersive Spectroscopy (EDS).

3. Results and Discussions

3.1. Oxide Ions Concentration Monitoring

The oxide ions anodic behaviour in LiCl-KCl at 550˚C was first studied by Li_2O additions using square wave voltammetry. Figure 1 presents square wave voltammograms performed at 81 Hz on a tungsten electrode for various O^{2-} quantities.

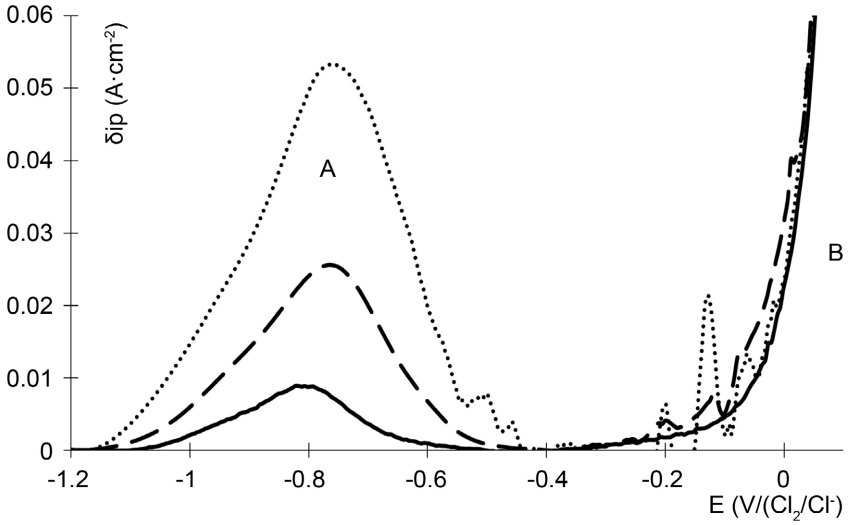

Figure 1. Square wave voltammograms in LiCl-KCl at 81 Hz after Li_2O additions, full line = no addition, dashes = addition of 0.0055 mol O^{2-} , dots = addition of 0.0116 mol O^{2-}, T = 550˚C, Working electrode: W, Counter electrode: W, Reference electrode: glassy carbon.

The exponential signal (B), observed at 0 V is associated with chloride ions

oxidation into chlorine gas and was used as an internal reference potential.

When Li_2O is added, a single anodic peak (A) is observed at −0.8 V/(Cl_2/Cl^-) and its corresponding peak current density increases with the addition of Li_2O: it is thus associated with the oxidation of O^{2-}. Despite the bubbling observed at higher anodic potentials (between −0.5 and 0 V/(Cl_2/Cl^-)), the shape of the peak is not disturbed, allowing an accurate measurement.

The differential peak current densities measured at −0.8 V/(Cl_2/Cl^-) are reported against O^{2-} concentration in Figure 2.

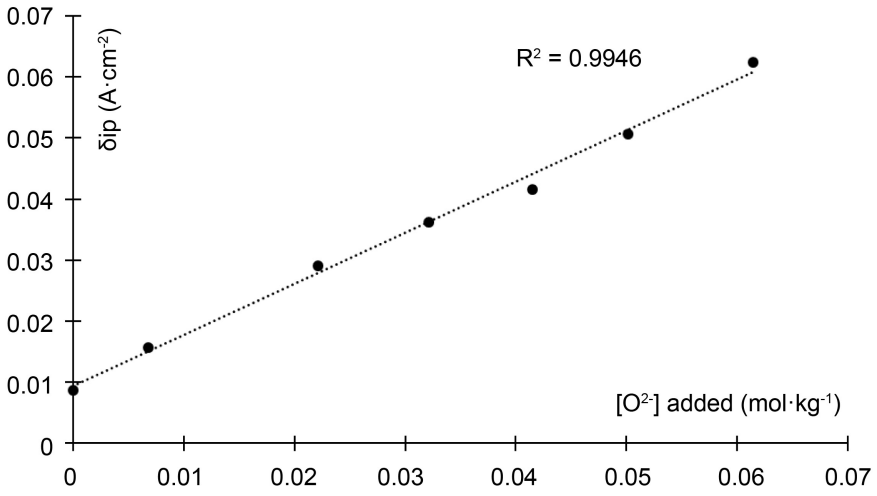

Figure 2. Calibration curve for O^{2-} titration, obtained by square wave voltammetry on a W electrode in the LiCl-KCl system at 550˚C. Frequency = 81 Hz.

A linear relationship is exhibited following the equation:

$$\delta ip = (0.85 \pm 0.04)\left[O^{2-}\right] + 0.0087 \quad (2)$$

where δip is the differential peak current density (A·cm^{-2}) and [O^{2-}] is the oxide ions molality in the salt (mol·kg^{-1}).

Using this linear relationship, the residual amount of oxide ions in the salt was estimated using the standard additions method to be around 0.01 mol·kg^{-1}. The slope of the calibration curve is 0.85 A·cm^{-2} (mol·kg^{-1})$^{-1}$ and was used to accurately quantify the oxide ions concentration in the salt before performing a corrosion experiment.

3.2. Influence of Oxide Ions on Material Behaviour

To investigate pure metals and SS316L behaviour in LiCl-KCl-Li_2O at 550˚C the same methodology was used. Linear sweep voltammetry were first performed in LiCl-KCl at 550˚C at different oxide ions concentrations, potential scan rates were determined and optimised to have the least effect on the reaction kinetics. To complete the linear sweep voltammetry results, pure metals were then immersed in a bath containing 0.150 mol O^{2-} kg^{-1} for 8 hours and SS316L for 168 hours in a bath containing 0.08 mol O^{2-} kg^{-1}. The immersed samples were then studied by

SEM-EDS analysis.

3.2.1. Chromium

Figure 3 gathers the linear sweep voltammograms obtained on a 2 mm diameter chromium rod for different oxide ions additions and the SEM micrography taken after immersion in LiCl-KCl at 550˚C.

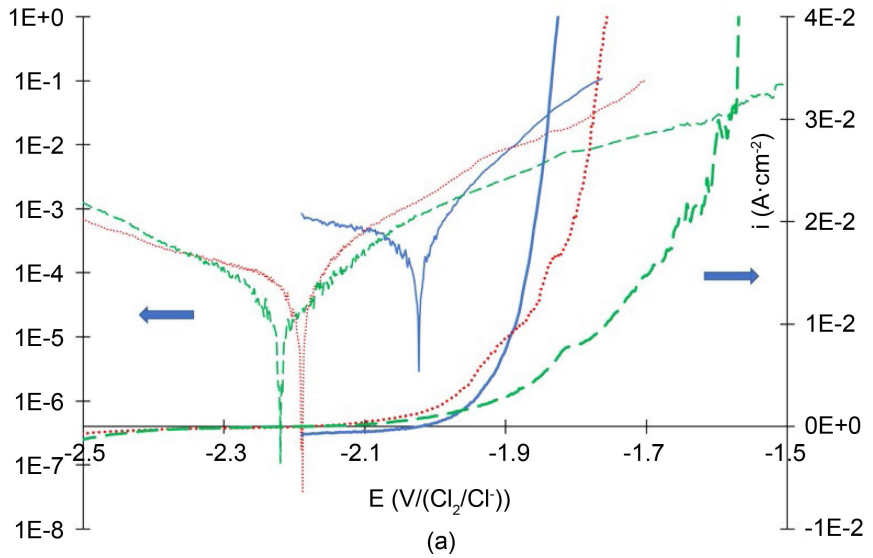

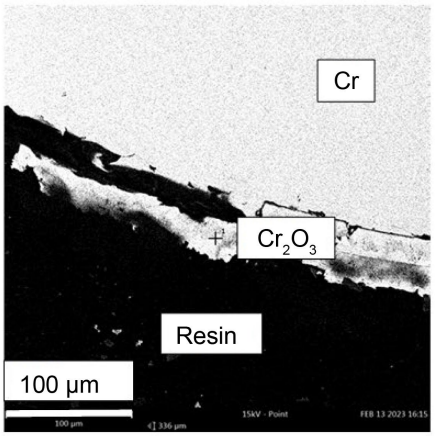

Figure 3. (a) Linear sweep voltammograms (0.5 $mV \cdot s^{-1}$) and their respective logarithmic representation on a 2 mm diameter chromium rod in LiCl-KCl at 550˚C at 0.003 mol O^{2-} kg^{-1} (blue full line), 0.025 mol O^{2-} kg^{-1} (red dots), 0.084 mol O^{2-} kg^{-1} (green dashes). (b) Cross section SEM micrography of a chromium rod immersed in LiCl-KCl at 550˚C for 8 hours. $[O^{2-}] = 0.150$ $mol \cdot kg^{-1}$.

Figure 3(a) displays three linear voltammograms and their logarithmic representations obtained on chromium for different oxide ions contents. An exponential increase in the current density is observed close to the open-circuit potential (OCP), indicating a corrosion phenomenon: thus, this potential can then be attri-

buted to the corrosion potential (E_{corr}). To better understand the Cr behaviour, logarithmic representations were used to accurately measure the corrosion potential and to estimate the corrosion rate.

For the lowest oxide ions content, chromium is directly dissolved into the bath. The oxide ions concentration increase leads to a decrease of both corrosion potential from −2.02 V/(Cl_2/Cl^-) to −2.22 V/(Cl_2/Cl^-) and corrosion rate from 3.4 10^{-4} A·cm^{-2} to 6 × 10^{-5} A·cm^{-2}: the oxide ions presence seems to stabilise the Cr metal. The formation of a protective layer on the electrode surface may be envisaged. To confirm it, an immersion test was performed and the sample analysed by SEM-EDS spot analysis (**Figure 3(b)**). Pure chromium is observed at the core, as well as a 50 µm-layer at the salt/metal interface. Elemental analyses showed an average molar composition of 38.5% Cr and 61.5% O, corresponding to Cr_2O_3.

Those results are in agreement with thermodynamic prediction regarding the spontaneous reaction between Cr and oxide ions. The Gibbs energy at 550˚C of Cr_2O_3 formation was calculated using the HSC 6.12 software:

$$2Cr + 1.5O_2 = Cr_2O_3 \qquad \Delta G^0_{550^\circ C} = -457\ \text{kJ}\cdot\text{mol}^{-1} \tag{3}$$

This highly negative value of the Gibbs energy indicates the Cr_2O_3 spontaneous formation in the presence of oxide ions when Cr and O^{2-} are simultaneously present in the salt.

Cr_2O_3 formation was already observed in different molten chloride salts [16] but was reported to be non-protective and easily dissolved [13].

3.2.2. Iron

The same methodology was applied to iron and **Figure 4** gathers the electrochemical signals and the SEM-EDS analysis.

The linear voltammograms (**Figure 4(a)**) exhibit three exponential signals towards the OCP showing a corrosion phenomenon whatever the oxide ions concentration. Moreover, no notable change is observed in the logarithmic representations in both corrosion potential (−1.86 V/(Cl_2/Cl^-)) and corrosion rate (around 4 × 10^{-4} A·cm^{-2}). Thus, oxide ions content has no influence on iron corrosion behaviour in LiCl-KCl at 550˚C.

The cross-sectional SEM micrography of the iron wire (**Figure 4(b)**) after the 8-hour immersion in LiCl-KCl ([O^{2-}] = 0.150 mol·kg^{-1}) shows a highly degraded salt/metal interface: a complementary EDS analysis was performed where only pure iron was observed. Thus, no protective oxide layer is formed and iron is dissolved in the molten solvent.

However, Feng and Melendres observed the formation of an unstable oxide film progressively dissolved by the chloride medium in molten LiCl-KCl at 450˚C in the presence of oxide ions ([17]. Thus, the following assumption can be made: the iron dissolution comes from either directly the metal oxidation or from the formation of an unstable Fe-O species.

3.2.3. Nickel

Figure 5 presents the experimental results obtained on a nickel wire.

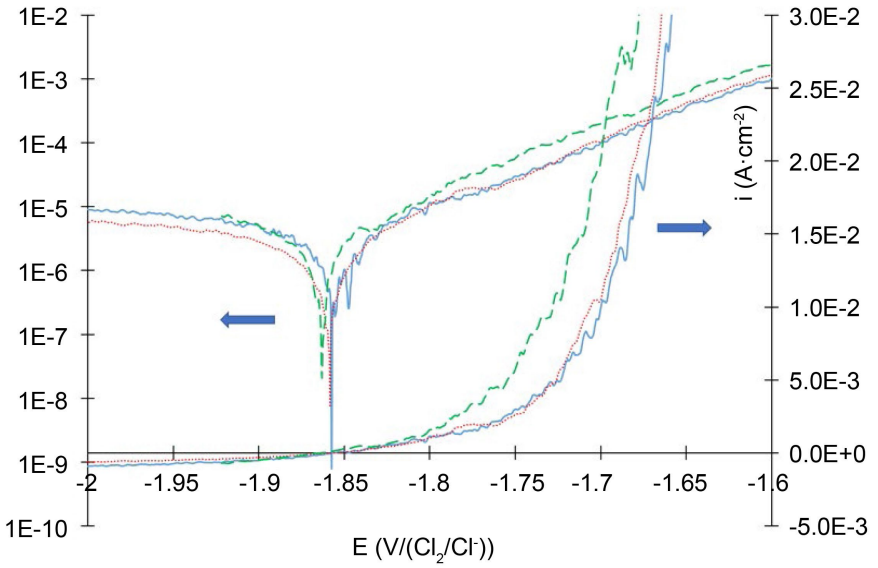

(a)

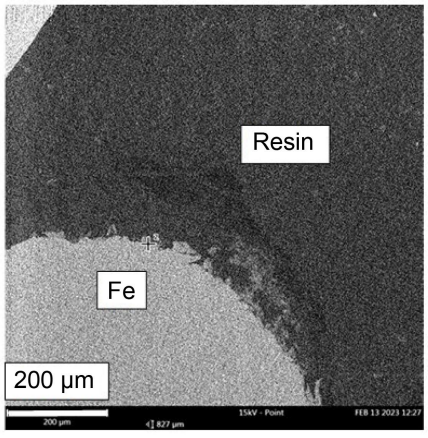

(b)

Figure 4. (a) Linear sweep voltammograms (0.5 mV·s^{-1}) and their respective logarithmic representation on a 1 mm diameter iron wire in LiCl-KCl at 550˚C at 0.004 mol O^{2-} kg^{-1} (blue full line), 0.026 mol O^{2-} kg^{-1} (red dots), 0.083 mol O^{2-} kg^{-1} (green dashes). (b) Cross section SEM micrography of an iron wire immersed in LiCl-KCl at 550˚C for 8 hours. [O^{2-}] = 0.150 mol·kg^{-1}.

The linear voltammograms show three exponentially-shaped signals obtained on a nickel wire where oxide ions content seems to have a low impact on the Ni behaviour (**Figure 5(a)**). The logarithmic representation gives new information compared to the sole linear voltammetry. As oxide ions concentration increases, $E_{i=0}$ drops from −1.53 V/(Cl_2/Cl^-) to −1.84 V/(Cl_2/Cl^-) while the exponential potential remains identical remains identical. A very low current density plateau (≈1 × 10^{-4} A·cm^{-2}) is observed in between, highlighting the corrosion resistance of nickel.

To confirm these results, an immersion test followed by SEM-EDS analysis was performed on nickel. The cross-sectional micrography taken after an 8-hour

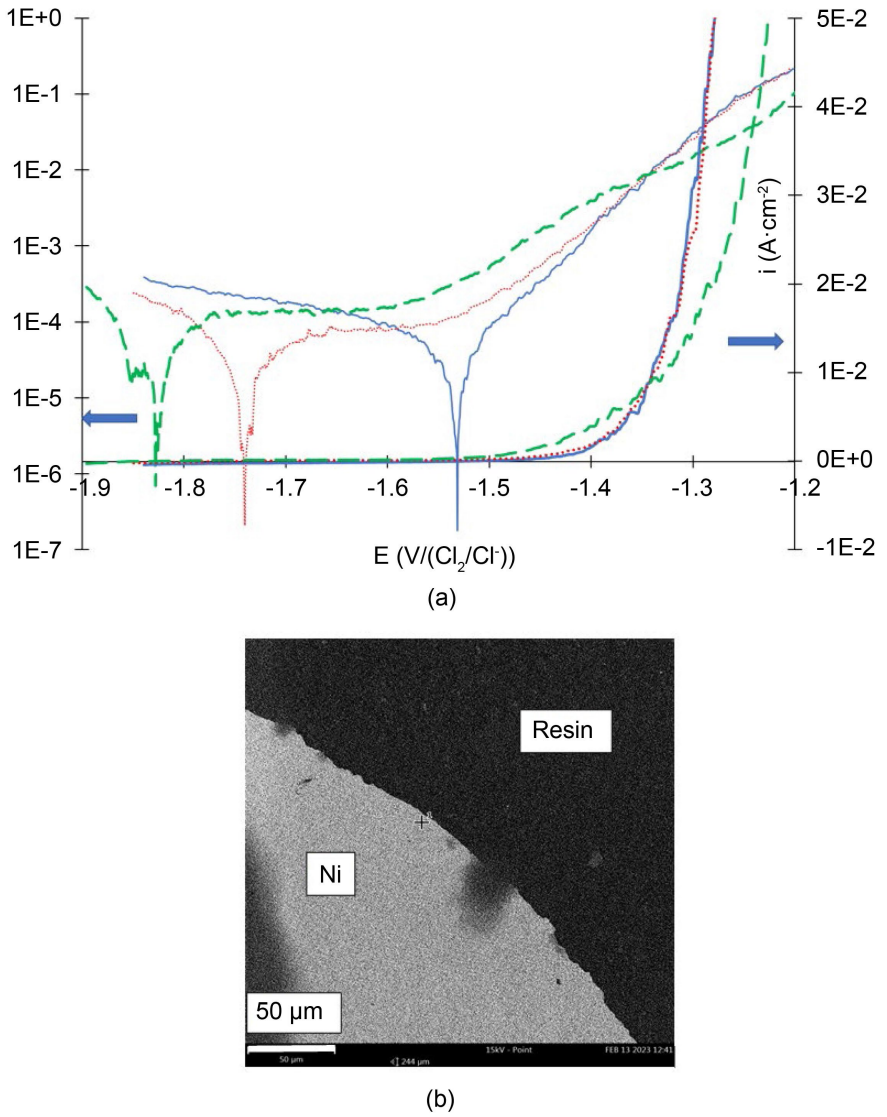

Figure 5. (a) Linear sweep voltammograms (1 mV·s^{-1}) and their respective logarithmic representation on a 1 mm diameter nickel wire in LiCl-KCl at 550˚C at 0.004 mol O^{2-} kg^{-1} (blue full line), 0.026 mol O^{2-} kg^{-1} (red dots), 0.084 mol O^{2-} kg^{-1} (green dashes). (b) Cross section SEM micrography of a nickel wire immersed in LiCl-KCl at 550˚C for 8 hours. [O^{2-}] = 0.150 mol·kg^{-1}.

immersion (**Figure 5(b)**) exhibits a nickel wire with an intact interface. EDS analysis was also performed and only pure Nickel was detected. Nickel is indeed resistant to corrosion and oxide ions have no influence on its behaviour, unlike Fe and Cr.

These observations are consistent with various studies showing a better corrosion resistance of nickel in molten chlorides compared to iron as an alloying compound [10] [18] [19].

3.2.4. Molybdenum

Figure 6 summarises the experiments carried out to study the influence of oxide

ions on a molybdenum wire.

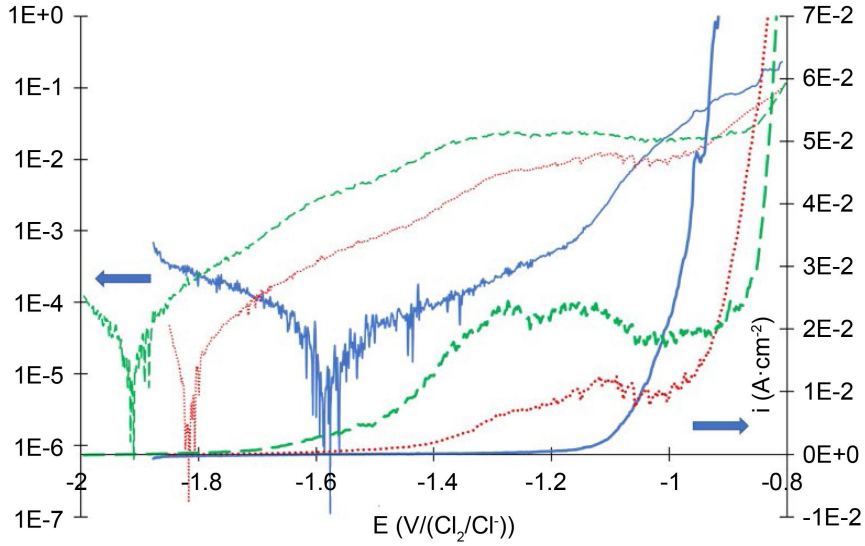

(a)

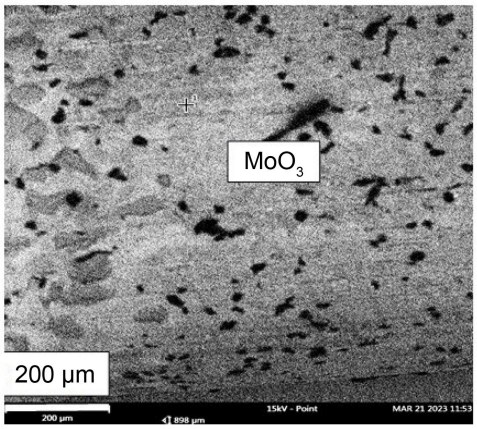

(b)

Figure 6. (a) Linear sweep voltammograms (1 $mV \cdot s^{-1}$) and their respective logarithmic representation on a 1 mm diameter molybdenum wire in LiCl-KCl at 550˚C at 0.004 mol O^{2-} kg^{-1} (blue full line), 0.026 mol O^{2-} kg^{-1} (red dots), 0.084 mol O^{2-} kg^{-1} (green dashes). (b) SEM micrography of a molybdenum wire immersed in LiCl-KCl at 550˚C for 8 hours. $[O^{2-}] = 0.150$ $mol \cdot kg^{-1}$.

The linear voltammograms plotted on molybdenum (**Figure 6(a)**) highlight the influence of oxide ions on the metal. For the low oxide ion molality (4×10^{-3} $mol \cdot kg^{-1}$), an exponential signal is observed on the linear voltammograms. However, on the logarithmic representation the corrosion potential is 0.6 V lower than the exponential and a low current density domain is present in between, thus Mo exhibits a corrosion resistance. With the oxide ions content increase, the corrosion potential decreases. Moreover, a new electrochemical signal is evidenced at -1.3 V/(Cl_2/Cl^-). Its peak current density is proportional to $[O^{2-}]$ and the signal is characteristic of a diffusion limited gas evolution, suggesting the formation of a

Mo-O gaseous species.

After immersion of a pure molybdenum wire in LiCl-KCl ($[O^{2-}]$ = 0.150 mol·kg^{-1}), EDS analysis showed an average molar composition of 72.3% oxygen and 27.7% molybdenum corresponding to MoO_3. According to the HSC 6.12 database, the formation of this oxide is spontaneous $\Delta G^0_{550^\circ C} = -535\ \text{kJ}\cdot\text{mol}^{-1}$.

MoO_3 was studied by Volkovicha *et al.* [14] in NaCl-KCl at 700˚C and observed that it reacted with NaCl to form gaseous MoO_2Cl_2. Thus, MoO_3 is spontaneously formed when Mo is in contact with O^{2-} and reacts with Cl^- to create a gaseous species, confirming the electrochemical observations. The oxide ions have then a negative effect on Mo corrosion behaviour.

3.2.5. Stainless Steel 316L

Finally, the same experiments were carried out on 316L stainless steel, the linear voltammograms are displayed in Figure 7.

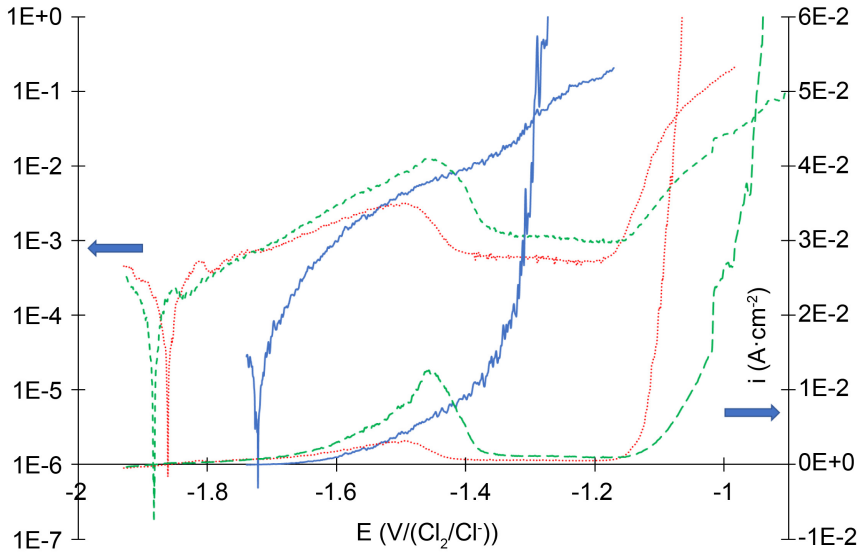

Figure 7. Linear sweep voltammograms (1 mV·s^{-1}) and their respective logarithmic representation on a 1 mm diameter SS316L wire in LiCl-KCl at 550˚C at 0.004 mol O^{2-} kg^{-1} (full line), 0.028 mol O^{2-} kg^{-1} (dots), 0.085 mol O^{2-} kg^{-1} (dashes).

The linear voltammograms and their logarithmic representations exhibit the complex behaviour of SS316L in the presence of oxide ions. When the O^{2-} content is low, 316L stainless steel shows a dissolution behaviour. Its corrosion potential is equal to −1.72 V/(Cl_2/Cl^-) and SS316L is thus unstable in a bath with low oxide ions content. As the oxide ions content increases, E_{corr} shifts from −1.72 to −1.9 V/(Cl_2/Cl^-). A new electrochemical signal emerged at $E \approx -1.45$ V/(Cl_2/Cl^-) followed by a low current density plateau ($i \approx 1 \times 10^{-3}$ A·cm^{-2}) between −1.4 and −1.15 V/(Cl_2/Cl^-). A shift of the exponential potential towards higher potentials is observed. These observations indicate the formation of a passivating compound.

A 168 h immersion of a 316L stainless steel plate in LiCl-KCl at 550˚C containing 0.081 mol O^{2-} kg^{-1} was then carried out. A micrograph was taken and a cross-

sectional element mapping was performed, results are presented on Figure 8.

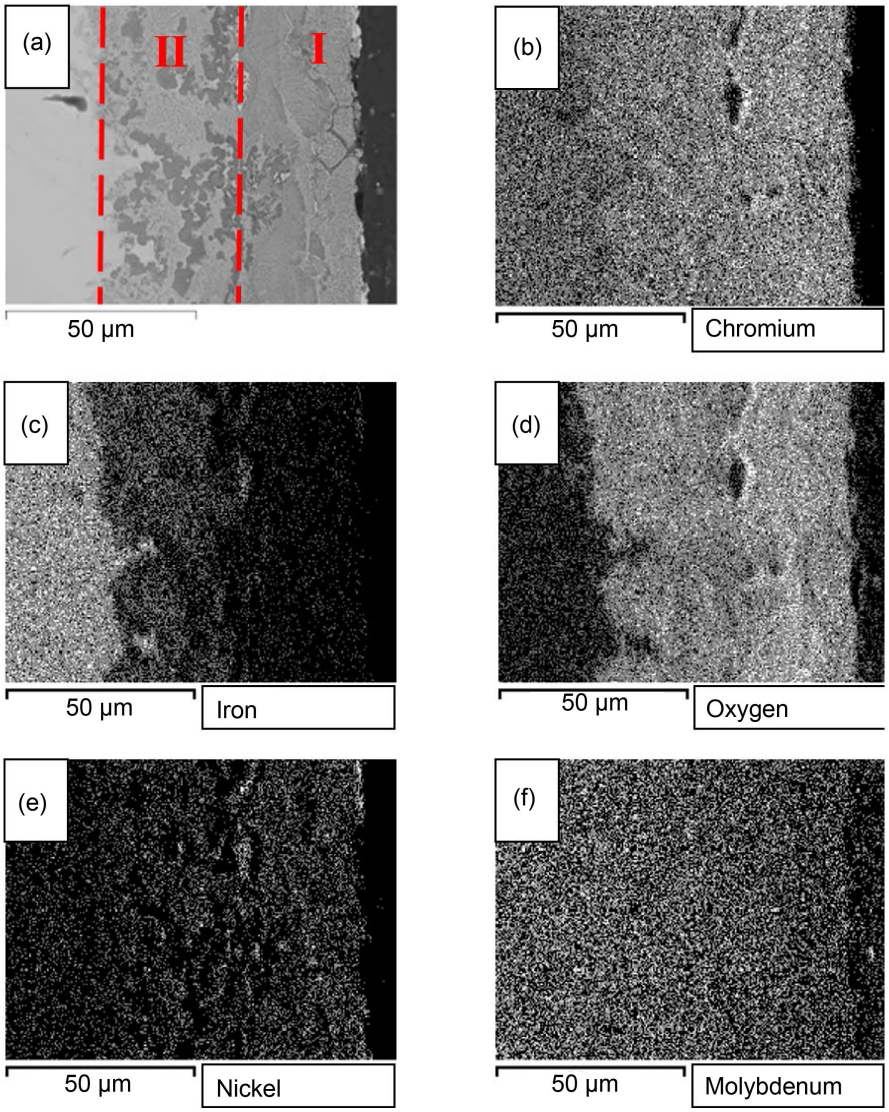

Figure 8. (a) Cross-sectional micrography of a 316L Stainless steel plate after a 168 hour immersion in an LiCl-KCl bath containing 0.081 mol O^{2-} kg^{-1} (T = 550˚C) and element mappings for (b) Chromium, (c) Iron, (d) Oxygen, (e) Nickel and (f) Molybdenum.

The SEM micrograph (Figure 8(a)) highlights the degradation of the alloy where a 75 µm-depth attack is observed after 168 h. Two distinct zones of attack can be identified, the first starting at the edge of the plate and reaching a depth of 35 µm (I symbol in Figure 8(a)), and the second one from 35 µm to 75 µm (II symbol on Figure 8(a)). This figure also displays the element mapping where a low concentration is symbolized by a darker colour and a high concentration is symbolized by a lighter colour.

The behaviour of alloying compound can be individually analysed and compared to its pure form.

Chromium is reactive towards oxygen and diffuses towards the interface where

its relative concentration increases (Figure 8(b)). Comparing Figure 8(b) and Figure 8(d), Cr is located next to the O element, confirming a spontaneous reaction.

Iron, main compound of the alloy (69%), diffuses towards the surface and dissolves into the bath (Figure 8(c)). In the zone I, the dissolution of iron reaches 90% of the original content. In the zone II, iron concentration is halved compared to its core composition. Iron in the alloy exhibits the same behaviour as its pure form.

Nickel was observed to be resistant to corrosion whatever the oxide concentration. During this immersion test, no depletion of nickel is observed (Figure 8(e)).

A slight depletion of Molybdenum is observed in the zone where O element is found (Figure 8(f)). The experiments conducted on pure molybdenum showed its spontaneous reactivity with oxides, first forming MoO_3, and then a gaseous MoO_2Cl_2 species, explaining the Mo depletion.

To resume, each alloying compound has the same behaviour as its pure form.

4. Conclusions

The experimental conditions control is essential in corrosion studies, in terms of atmosphere and impurities, especially oxide ions. This work focused on the development of a titration method to determine oxide ions concentration in the salt, based on SWV on a W electrode.

Then, stainless steel 316L and its pure alloying compounds were studied in LiCl-KCl-Li_2O at 550˚C by electrochemical measurements and by immersions followed by SEM-EDS analysis at various oxide ions content. The results obtained on each material showed the importance of oxide ions monitoring as it can drastically change the behaviour of an element.

On pure metals, chromium was found to be spontaneously dissolved in the bath when oxide ions concentration was low. As it increased, the formation of a Cr_2O_3 layer was observed, slowing down the corrosion rate of the metal. Iron was spontaneously dissolved in the bath whatever the oxide ions concentration whereas nickel was resistant to corrosion independently of oxide ions concentration. Molybdenum was found resistant to corrosion when O^{2-} content was low. When $[O^{2-}]$ increased, the formation of an unstable layer of MoO_3 was observed, leading to a gaseous MoO_2Cl_2 species.

The electrochemical study of SS316L showed a dissolution behaviour for low O^{2-} content. As oxide ions concentration increased, a passivation layer was observed and visually confirmed by SEM-EDS after a 168 h immersion test. Each alloying element composing the SS316L showed consistent behaviour with its pure form.

Conflicts of Interest

The authors declare no conflicts of interest regarding the publication of this paper.

References

[1] Kelly, J.E. (2014) Generation IV International Forum: A Decade of Progress through International Cooperation. *Progress in Nuclear Energy*, **77**, 240-246. https://doi.org/10.1016/j.pnucene.2014.02.010

[2] Ladkany, S., Culbreth, W. and Loyd, N. (2018) Molten Salts and Applications I: Molten Salt History, Types, Thermodynamic and Physical Properties, and Cost. *Journal of Energy and Power Engineering*, **12**, 507-516. https://doi.org/10.17265/1934-8975/2018.11.001

[3] Manly, W.D., Adamson, G.M. and Douglas, D.A. (1958) Aircraft Reactor Experiment Metallurgical Aspects.

[4] Cottrell, W.B., Hungerford, H.E., Leslie, J.K. and Meem, J.L. (1955) Operation of the Aircraft Reactor Experiment. https://doi.org/10.2172/4237975

[5] Lane, J.A., MacPherson, H.G. and Maslan, F. (1958) Fluid Fuel Reactors: Molten Salt Reactors, Aqueous Homogeneous Reactors, Fluoride Reactors, Chloride Reactors, Liquid Metal Reactors and Why Liquid Fission. Addison-Wesley Publications.

[6] Bhabha Atomic Research Centre (2015) Proceedings of the International Thorium Energy Conference: Gateway to Thorium Energy, Mumbai, 12-15 October 2015, 637.

[7] Lewitz, J.-C., *et al*. (2020) The Dual Fluid Reactor—An Innovative Fast Nuclear-Reactor Concept with High Efficiency and Total Burnup. *Research and Innovation*, **65**, 1-10.

[8] Kramer, K., *et al*. (2018) Terra Power's Molten Chloride Fast Reactor Technology. https://doi.org/10.13140/RG.2.2.18467.09768

[9] Slusser, J.W., Titcomb, J.B., Heffelfinger, M.T. and Dunbobbin, B.R. (1985) Corrosion in Molten Nitrate-Nitrite Salts. *JOM*, **37**, 24-27. https://doi.org/10.1007/bf03259692

[10] Ding, W., Shi, H., Xiu, Y., Bonk, A., Weisenburger, A., Jianu, A., *et al*. (2018) Hot Corrosion Behavior of Commercial Alloys in Thermal Energy Storage Material of Molten $MgCl_2$/KCl/NaCl under Inert Atmosphere. *Solar Energy Materials and Solar Cells*, **184**, 22-30. https://doi.org/10.1016/j.solmat.2018.04.025

[11] Sun, H., Wang, J., Li, Z., Zhang, P. and Su, X. (2018) Corrosion Behavior of 316SS and Ni-Based Alloys in a Ternary NACl-KCl-$MgCl_2$ Molten Salt. *Solar Energy*, **171**, 320-329. https://doi.org/10.1016/j.solener.2018.06.094

[12] Shankar, A.R., Kanagasundar, A. and Mudali, U.K. (2013) Corrosion of Nickel-Containing Alloys in Molten LiCl-KCl Medium. *Corrosion*, **69**, 48-57. https://doi.org/10.5006/0627

[13] Ishitsuka, T. and Nose, K. (2002) Stability of Protective Oxide Films in Waste Incineration Environment—Solubility Measurement of Oxides in Molten Chlorides. *Corrosion Science*, **44**, 247-263. https://doi.org/10.1016/s0010-938x(01)00059-2

[14] Volkovicha, V.A., Griffiths, T.R., Thied, R.C. and Lewin, B. (2003) Behavior of Molybdenum in Pyrochemical Reprocessing: A Spectroscopic Study of the Chlorination of Molybdenum and Its Oxides in Chloride Melts. *Journal of Nuclear Materials*, **323**, 93-100. https://doi.org/10.1016/j.jnucmat.2003.08.039

[15] Massot, L., Cassayre, L., Chamelot, P. and Taxil, P. (2007) On the Use of Electrochemical Techniques to Monitor Free Oxide Content in Molten Fluoride Media. *Journal of Electroanalytical Chemistry*, **606**, 17-23. https://doi.org/10.1016/j.jelechem.2007.04.005

[16] Lehmusto, J., Skrifvars, B., Yrjas, P. and Hupa, M. (2011) High Temperature Oxidation

of Metallic Chromium Exposed to Eight Different Metal Chlorides. *Corrosion Science*, **53**, 3315-3323. https://doi.org/10.1016/j.corsci.2011.06.007

[17] Feng, X.K. and Melendres, C.A. (1982) Anodic Corrosion and Passivation Behavior of Some Metals in Molten LiCl-KCl Containing Oxide Ions. *Journal of the Electrochemical Society*, **129**, 1245-1249. https://doi.org/10.1149/1.2124095

[18] Ambrosek, J.W. (2011) Molten Chloride Salts for Heat Transfer in Nuclear Systems.

[19] Vignarooban, K., Xu, X., Wang, K., Molina, E.E., Li, P., Gervasio, D., *et al*. (2015) Vapor Pressure and Corrosivity of Ternary Metal-Chloride Molten-Salt Based Heat Transfer Fluids for Use in Concentrating Solar Power Systems. *Applied Energy*, **159**, 206-213. https://doi.org/10.1016/j.apenergy.2015.08.131